HHS Public Access

Author manuscript

Dev Biol. Author manuscript; available in PMC 2017 April 15.

Published in final edited form as:

Dev Biol. 2016 April 15; 412(2): 219–233. doi:10.1016/j.ydbio.2016.02.029.

Protein tyrosine kinase 7 is essential for tubular morphogenesis of the Wolffian duct

Bingfang Xu[a], **Angela M. Washington**[a], **Raquel Fantin Domeniconi**[a,b], **Ana Cláudia Ferreira Souza**[a,c], **Xiaowei Lu**[a], **Ann Sutherland**[a], and **Barry T. Hinton**[a,*]

[a]Department of Cell Biology, University of Virginia School of Medicine, Charlottesville, USA

[b]Department of Anatomy, Institute of Biosciences – UNESP, Botucatu, Brazil

[c]Department of General Biology, Federal University of Viçosa, Viçosa, Brazil

Abstract

The Wolffian duct, the proximal end of the mesonephric duct, undergoes non-branching morphogenesis to achieve an optimal length and size for sperm maturation. It is important to examine the mechanisms by which the developing mouse Wolffian duct elongates and coils for without proper morphogenesis, male infertility will result. Here we show that highly proliferative epithelial cells divide in a random orientation relative to the elongation axis in the developing Wolffian duct. Convergent extension (CE)-like of cell rearrangements is required for elongating the duct while maintaining a relatively unchanged duct diameter. The Wolffian duct epithelium is planar polarized, which is characterized by oriented cell elongation, oriented cell rearrangements, and polarized activity of regulatory light chain of myosin II. Conditional deletion of protein tyrosine kinase 7 (PTK7), a regulator of planar cell polarity (PCP), from mesoderm results in loss of the PCP characteristics in the Wolffian duct epithelium. Although loss of Ptk7 does not alter cell proliferation or division orientation, it affects CE and leads to the duct with significantly shortened length, increased diameter, and reduced coiling, which eventually results in loss of sperm motility, a key component of sperm maturation. In vitro experiments utilizing inhibitors of myosin II results in reduced elongation and coiling, similar to the phenotype of Ptk7 knockout. This data suggest that PTK7 signaling through myosin II regulates PCP, which in turn ensures CE-like of cell rearrangements to drive elongation and coiling of the Wolffian duct. Therefore, PTK7 is essential for Wolffian duct morphogenesis and male fertility.

Keywords

Ptk7; tubular morphogenesis; Wolffian duct; planar cell polarity; male infertility

Correspondence and reprint requests to: Barry T. Hinton, Ph.D., Department of Cell Biology, University of Virginia Health System, PO Box 800732, Charlottesville, VA 22908, USA, Tel: 434-924-2174, Fax: 434-982-3912, bth7c@virginia.edu.

Author contributions

B.X. and B.T.H. designed research and analyzed data and wrote the paper; B.X., A.M.W, R.F.D., and A.C.F.S. performed research; X.L. and A.S. contributed new reagents/analytic tools and provided guidance and help with experimental design.

1. Introduction

Tubulogenesis is a highly conserved process, from Drosophila to mammals, with each tube having a specific role tailored to the needs of that organ/organism (Andrew and Ewald, 2010; Iruela-Arispe and Beitel, 2013; Lubarsky and Krasnow, 2003). It is clear that the formation of tubes in many tissues arises through a variety of unique processes, e.g. wrapping and budding. Once that tube has formed, it then undergoes a series of morphogenic events to generate a tissue/organ of the correct length, shape, and size to fulfill its function. Failure to do so results in the failure of that tissue/organ to function properly. The mesonephric/nephric duct has been well studied from the perspective of kidney morphogenesis (Carroll and Yu, 2012; Karner et al., 2009; Kobayashi et al., 2005; Lienkamp et al., 2012; Schnell and Carroll, 2014), which is an excellent example of branching morphogenesis. However, the cranial portion of the mesonephric duct gives rise to the Wolffian duct, the precursor of the epididymis, which is formed via non-branching morphogenesis. Morphogenesis of the Wolffian duct is not trivial in that this duct will eventually elongate to over 1 m in the mouse and 6 m in the human (Hinton et al., 2011), and folds extensively to form an organ of approximately 1 cm and 6–7 cm long, respectively. Undergoing the morphogenic events will ensure that the Wolffian duct is of the proper length and size for sperm maturation, which is critical for male fertility.

Tubular morphogenesis can occur by several mechanisms including cell proliferation, cell rearrangements, cell shape change, and cell recruitment (Andrew and Ewald, 2010). It is unclear which cellular mechanisms underlie Wolffian duct morphogenesis. We hypothesized that cell proliferation was a major contributor (Hinton et al., 2011; Sun and Flickinger, 1982; Xu et al., 2010) and that orientated cell divisions may lengthen the duct and maintain duct diameter. In addition, the Wolffian duct may also elongate via convergent extension (CE)-like of cell rearrangements and cell shape change. However, cell recruitment is not a major contributor, at least during the embryonic period, because cells identified as originating from the mesenchyme were not observed in the Wolffian duct epithelium (Mugford et al., 2008).

Polarity of cells is often described along the apical-basal axis, but polarity also exists within the plane of the epithelium of that tissue or organ. This type of polarity is referred to as planar cell polarity (PCP). PCP mechanisms play an important role during the development of many organs across many species. Specifically, PCP is required for both CE and oriented cell divisions in several tissues (Karner et al., 2009; Williams et al., 2014; Yen et al., 2009; Yu et al., 2009). Therefore, it is further hypothesized that PCP mechanisms contribute to Wolffian duct morphogenesis.

Protein tyrosine kinase 7 (PTK7), a receptor tyrosine kinase-like molecule, acts as an important regulator of PCP (Hayes et al., 2013; Lu et al., 2004). PTK7 regulates neural tube closure, stereociliary bundle orientation, polarized cell motility, and CE during gastrulation and neurulation (Lu et al., 2004; Williams et al., 2014; Yen et al., 2009). Genetic evidence suggests that PTK7 regulates myosin II activity and PCP orientation in auditory sensory epithelium and neural plate (Andreeva et al., 2014; Lee et al., 2012; Williams et al., 2014).

PTK7 is therefore, considered to be a prime candidate in regulating Wolffian duct morphogenesis.

Taken together, our working hypothesis is that PTK7 regulates Wolffian duct morphogenesis through cell proliferation coupled with CE-like of cell rearrangements driven by myosin II activation. This allows the duct to be optimal in length and size for sperm maturation and therefore, male fertility.

2. Results

2.1. Ptk7 mutant shows abnormal development of the Wolffian duct

$Ptk7^{Xst87/Xst87}$ mice, which are homozygous for the gene-trap allele Xst87 (Lu et al., 2004), had a shortened Wolffian duct and an unusual coiling pattern compared to controls at embryonic day 18.5 (E18.5) (Fig. 1A–B). Unfortunately, $Ptk7^{Xst87/Xst87}$ mice die perinatally due to a craniorachischisis phenotype. Therefore, T-Cre (Perantoni et al., 2005) and a "floxed" Ptk7 allele (Lee et al., 2012) were employed to conditionally knockout (cKO) Ptk7 from the mesoderm. Pan-mesoderm loss of Ptk7 ($Ptk7^{flox/Xst87}$:$T\text{-}Cre^{tg}$, namely TCre-cKO) resulted in spina bifida in an incompletely penetrant manner. The majority of mice with spina bifida died shortly after birth. However, a significant proportion of TCre-cKO mice did not exhibit spina bifida, but instead had a coiled tail and survived to adulthood.

Similar to $Ptk7^{Xst87/Xst87}$, Wolffian ducts of TCre-cKOs were shorter and less coiled compared to controls at E18.5 (Fig. 1C–D), and the ducts had increased diameter compared to controls at postnatal day 14 (P14) and at the adult stage (Fig. 1E–H). In adults, TCre-cKOs often developed blockages in the seminiferous tubules, which resulted in epididymal regression. Spermatozoa were absent from those epididymides, and these regressed epididymides were excluded from our experiments. When blockage was not present in TCre-cKO testes, spermatozoa could be collected from the cauda. Those spermatozoa had very low (<1%) motility. In contrast, spermatozoa from control mice moved progressively when placed into a culture medium (Movies S1 and S2). The weight of the seminal vesicle from these adult knockout mice (229.3 ± 78.2 mg) (mean ± SEM) was not significantly different from litter mate controls (241.9 ± 39.3 mg).

The reduction in length and coiling in TCre-cKOs could not be rescued using an in vitro organ culture with testosterone supplementation (Movies S3 and S4). E15.5 TCre-cKO ducts elongated much slower than controls in a 72h culture (Fig. 1I). As shown in Fig. S1, control ducts increased 44.1% in length and added 3.6 additional bends on average during the first 24h while TCre-cKO ducts only increased 6.4% in length and did not show bends. Control ducts began 3D coiling from 48h onwards while TCre-cKO ducts only showed 2D coiling after 72h of culture (Fig. 1I).

2.2 Loss of Ptk7 resulted in an increase in duct diameter

A morphological study revealed that E18.5 TCre-cKO Wolffian ducts had increased diameter and increased epithelial cell number at the circumference. TCre-cKO ducts were wrapped by more layers of mesenchymal cells compared to controls at E18.5. The morphological changes due to loss of Ptk7 became more apparent at P7. At P14, the

knockout epithelium underwent pseudo-stratification in contrast to the simple epithelium in controls (Fig. 2A). Labeling of membrane protein CDH2 (cadherin 2) demonstrated that epithelial cells stacked upon each other (Fig. 3A–B). In addition, mesenchymal cells surrounding the epithelium in P14 TCre-cKOs were not as elongated compared to controls (Fig. 2A, arrows). When spermatozoa entered the epididymis in adult mice, dilation of the duct in TCre-cKOs was observed (Fig. 2A). Statistical analysis revealed duct diameter and epithelial cell number per cross-section of the duct increased significantly following loss of Ptk7 at all examined ages (Fig. 2B, $p<0.01$).

Despite the dramatic changes in morphology, TCre-cKO ducts maintained normal epithelial characteristics. Apical labeling of APKC (atypical protein kinase C), a marker for apical-basal polarity of the epithelium, was normal in TCre-cKOs (Fig. 3C–D). COL4 (collagen 4) was localized to the basolateral membrane of a subset of epithelial cells in controls and TCre-cKOs. In addition, labeling of COL4 at the basement membrane of the epithelium was thicker in TCre-cKOs compared to controls, but was intact in both control and TCre-cKO ducts (Fig. 3E–F). Labeling intensity of androgen receptor (AR) in the epididymides was similar between controls and TCre-cKOs at P14 (Fig. 3G–H).

2.3 PTK7 localization changed dynamically during Wolffian duct development

Loss of Ptk7 affected morphology of the epithelium and surrounding mesenchyme, therefore, PTK7 localization was investigated. In control mice, PTK7 was localized to the basolateral plasma membrane of epithelial cells and the entire plasma membrane of mesenchymal cells at embryonic and early postnatal stages (Fig. 4A–B). During these stages, labeling intensity of PTK7 was highest at the plasma membrane of mesenchymal cells closely surrounding the epithelium (Fig. 4A–B). However, from P14 onwards, higher labeling intensity of PTK7 was found at the basolateral plasma membrane of epithelial cells compared to mesenchymal cells (Fig. 4C–D). Deletion of PTK7 in TCre-cKOs was confirmed by immunofluorescent analysis. Compared to controls, PTK7 labeling was absent from the plasma membrane of epithelial and mesenchymal cells in TCre-cKOs. Punctate labeling from the gene-trap Ptk7 allele (Xst87) was observed in knockout tissues (Fig. 4E, white arrow).

2.4 Loss of Ptk7 from smooth muscle cells and epithelial cells showed different phenotypes

To study the distinct roles of Ptk7 in epithelial cells and mesenchymal cells, three conditional knockout models were established. 1) Ptk7 was conditionally removed from epithelial cells in the most proximal regions of the epididymis from P17 onwards using Rnase10-Cre (Krutskikh et al., 2011) ($Ptk7^{flox/Xst87}$:$Rnase10\text{-}Cre^{tg}$, namely, RnCre-cKO); 2) Ptk7 was conditionally removed from epithelial cells in most epididymal regions except for the initial segment from embryonic stage onwards using Hoxb7-Cre (Yu et al., 2002) ($Ptk7^{flox/Xst87}$:$Hoxb7\text{-}Cre^{tg}$, namely, HoxCre-cKO; 3) Ptk7 was conditionally removed from smooth muscle cells from embryonic stage onwards using Sm22-Cre (Yoshida et al., 2010) ($Ptk7^{flox/Xst87}$:$Sm22\text{-}Cre^{tg}$, namely, SmCre-cKO). Recombination efficiency of Hoxb7-Cre and Rnase10-Cre in the Wolffian duct was examined previously (Xu et al., 2013). Recombination efficiency of SM22-Cre was tested in this study by breeding Cre mice with

mT/mG Cre reporter mice. Recombination driven by Sm22-Cre is completed in smooth muscle layers of the mesenchyme at E18.5 (Fig. S2).

When Ptk7 was removed from epithelial cells of the initial segment, dilation of the duct was observed (Fig. 5A). Duct diameter and number of epithelial cells per cross-section of the duct in adult RnCre-cKO initial segments increased significantly compared to controls (Fig. 5B). Similarly, dilation of the duct was observed in the caput of HoxCre-cKO epididymides (Fig. 5). By contrast, overall morphology of SmCre-cKO epididymides did not display differences compared to controls in adults (Fig. 5A). Morphological changes due to loss of Ptk7 in HoxCre-cKOs and RnCre-cKOs were limited to epididymal regions where Ptk7 was removed, and the changes were not as severe as TCre-cKOs. Therefore, the TCre-cKO was used to study the mechanisms that underlie the knockout phenotype.

2.5 Loss of Ptk7 did not affect cell proliferation and randomly oriented cell division in the epithelium

Despite a shorter Wolffian duct following loss of Ptk7, cell proliferation in all four epididymal regions did not show significant differences in TCre-cKOs at P14 compared to controls (Fig. 6A). Apoptosis was rarely observed in both controls and TCre-cKOs (Fig. 3I–J).

To investigate cell division orientation of epithelial cells and its contribution to elongation of the Wolffian duct, the angle of mitotic spindle relative to the axis of duct elongation in relatively straight E15.5 ducts was measured (Fig. S3A). As shown in Fig. 6B, cell division was randomly oriented in both E15.5 controls and TCre-cKOs. The distributions of division orientation in both E15.5 controls and TCre-cKOs were not significantly different from predicted random distribution (KS test).

From E15.5 onwards, the Wolffian duct underwent dramatic coiling. The convoluted nature of the duct prevented us from accurately measuring mitotic spindle orientation, therefore, an alternative approach was used. As shown in Fig. S3B–I, mitotic spindles were visualized in the tissue sections from P14 epididymides. Division orientation was estimated in either cross-sections, being a perfect circle (Fig. S3B–D), or in longitudinal sections along the axis of the duct (Fig. S3E–H). Examining division orientation of 453 and 121 epithelial cells in P14 controls and TCre-cKOs, respectively, ~50% were estimated to orient 45–90 degrees to the duct axis while another ~50% were 0–45 degrees (Fig. 6C).

2.6 Loss of Ptk7 disrupted PCP in the epithelium of the Wolffian duct

To determine whether the epithelium of the Wolffian duct is planar polarized, cell shape of epithelial cells was analyzed at E18.5 using membrane EGFP (Fig. 7, Table S1). In controls, at basal ends of epithelial cells, >90% of cells showed polarized elongation. Among elongated cells, >85% of them were oriented between 45–90 degrees (perpendicular) to the axis of duct elongation. Moreover, >65% of elongated cells were oriented within 70–90 degrees (Fig. 7A and D). In TCre-cKOs, fewer cells, 77%, exhibited polarized elongation at basal ends compared to controls, and elongated cells showed randomized elongation. ~50% were elongated within 45–90 degrees and ~30% within 70–90 degrees (Fig. 7A and D). Statistical analysis shows there is a significant difference in the orientation of cell elongation

at basal ends between controls and TCre-cKOs ($p<0.001$, KS test). In addition, high percentages of epithelial cells were not elongated at their apical ends, and elongated cells were not mediolaterally aligned in both knockouts and controls (Fig. 7A and C). Apical constriction, which was required to maintain the shape of a duct, was observed in both control and TCre-cKO ducts (Fig. 7B). The ratios of basal area vs. apical area were 2.8 in control cells and 3.4 in TCre-cKO cells. The height of epithelial cells was not significantly different between controls and TCre-cKOs. However, lumen diameter of TCre-cKOs significantly increased compared to controls (Fig. 7B, Table S1).

2.7 Loss of Ptk7 disrupted oriented cell rearrangements at mid-levels of epithelial cells

Epithelial cells in the Wolffian duct were tall with average cell height vs. length at basal ends being 1.9 and 2.4 times in controls and TCre-cKOs, respectively (Fig. 7B, Table S1). In examining cell clusters through Z-stack images of the Wolffian duct, evidence for cell rearrangements was found between apical and basal ends of cell clusters in both controls and TCre-cKOs at E18.5. Note that we were unable to follow these rearrangements in real time due to the difficulty of imaging the ducts at high resolution under the culture conditions required for duct elongation. However, analysis of cell organization in freshly dissected ducts provided clear evidence for at least three different cell rearrangements: T1 process, rosette resolution, and single cell intercalation (Fig. 8A).

T2 (four cells with a common vertex) and rosette (five or more cells with a common vertex) structures were found approximately half way between apical and basal ends of cell clusters in controls and TCre-cKOs. This location was defined as the mid-level (Fig. S4A–B). As shown in the diagram (Fig. S4A), the most common type of T1 process in controls was that a cluster of four cells showed a mediolateral neighbor contact (T3) towards apical ends, T2 structure at mid-levels, and a neighbor contact along the elongation axis (T1) towards basal ends. This type was named as T3-T2-T1. The most common type of rosette resolution in controls was that five or more cells formed an elongation-axis-oriented array towards apical ends, a rosette structure at mid-levels, and a mediolateral-oriented array towards basal ends. This type was named as E-R-M. In T3-T2-T1 and E-R-M, two adjacent cells shown in white along the elongation axis at basal ends became separated at apical ends (Fig. 8A). In controls, T3-T2-T1 and E-R-M accounted for ~70% of the examples of T1 process and rosette resolution, respectively (Fig. 8B). However, in TCre-cKOs, T2 and rosettes resolved to more random patterns of cell-cell association towards apical and basal ends, and T3-T2-T3 and E-R-E were the most common types, in which two cells shown in white along the elongation axis joined at mid-levels but were separated in both apical and basal ends (Fig. 8).

In regards to single cell intercalation, we observed many groups of cells where the apical region of a cell was intercalated between two cells while its basal region remained alongside these two adjacent cells. The most common type of single cell intercalation in both controls and TCre-cKOs was that the apical region of cells inserted between two adjacent cells that lay along the elongation axis (namely Y type; Fig. 8A). However, the percentage of X type, an insertion between two adjacent cells that lay along the circumference of the duct, was higher in TCre-cKOs compared to controls (Fig. 8). The frequency of T1 process, rosette

resolution, and single cell intercalation was similar among controls and TCre-cKOs (Fig. S4C).

2.8 Loss of Ptk7 impaired polarized myosin II localization in the Wolffian duct

Polarized localization of myosin II underlies PCP and CE (Lienkamp et al., 2012; Williams et al., 2014). Therefore, we analyzed the localization of myosin II regulatory light chain phosphorylated at Ser19 (pRLC), a marker for myosin contractility (Vicente-Manzanares et al., 2009). Optical cross-sections at basal ends of epithelial cells in control E15.5 epididymides showed that pRLC was preferentially localized at the cell boundary perpendicular to the duct axis (Fig. 9A, arrows). The ratio of labeling intensity at the cell boundaries perpendicular vs. parallel to the duct axis was approximately 2:1 (Fig. 9B). This polarized localization pattern persisted in mid-levels of epithelial cells (Fig. 9A–B, arrows). Although the apical junction had strong pRLC labeling, a polarized distribution was not observed in either controls or TCre-cKOs (Fig. 9A–B). The polarized localization of pRLC was diminished at basal ends and mid-levels of epithelial cells in TCre-cKOs. Instead, pRLC was localized at the joined points of multiple cell boundaries (Fig. 9A, arrowheads). The ratio of labeling intensity at the cell boundaries perpendicular vs. parallel to the duct axis was approximately 1:1 at basal ends and mid-levels in TCre-cKOs (Fig. 9B).

2.9 Myosin II inhibitors suppressed elongation and coiling of the Wolffian duct

When wild-type E16.5 Wolffian ducts were incubated with blebbistatin, an inhibitor of myosin activity, duct elongation and coiling decreased. As shown in Fig. 10, the effects of inhibition were visible at 5h. After 24h, duct coiling was significantly affected by 2.5 μM or 5 μM blebbistatin. However, elongation was significantly affected only at the higher dose (5 μM) (Fig. 10B). The effects of inhibition were reversed upon inhibitor withdrawal.

ROCK1/2 are known as myosin II activators (Wilkinson et al., 2005). When wild-type E16.5 Wolffian ducts were incubated with Y27632, an inhibitor of ROCK1/2, myosin activity was measured by changes in the degree pRLC intensity. As shown in Fig. S5, pRLC labelling intensity declined slightly in the basolateral membrane of epithelial cells. Unlike being localized to multiple layers of smooth muscle cells in controls, pRLC labelling was localized to a single layer of muscle cells adjacent to the epithelial duct. Inhibitory effects of Y27632 on elongation and coiling were similar but slightly different compared to blebbistatin. When wild-type E16.5 Wolffian ducts were incubated with 1 μM or 2.5 μM Y27632, the inhibitory effect became significant after the first 24h of incubation, as shown by significantly decreased elongation and coiling (Fig. 11B). At 48h, a higher dose (2.5 μM) Y27632 showed stronger inhibitory effects on duct coiling and elongation compared to a lower dose (1 μM). The effects of inhibition were reversed upon inhibitor withdrawal (Fig. 11).

3. Discussion

To achieve the optimal shape, size and length of a tubular organ, and therefore function, a series of complex and highly regulated morphogenic events over time are necessary. Wolffian duct morphogenesis is no exception. It undergoes a rapid transformation from a straight duct to a highly coiled segmented organ of the proper length and shape such that it

can function to allow sperm maturation to take place, which is critical for male fertility (Xu et al., 2014). Clinically, failure of the human vas deferens to develop appropriately and failure of the tubules of the caput region to reach the testis, epididymal disjunction, are failures of the Wolffian duct and mesonephric tubules respectively to undergo normal morphogenesis. Interestingly, a study has shown that 30–79% of boys with an undescended testis also showed Wolffian duct abnormalities of which 25% displayed epididymal disjunction (Girgis et al., 1969; Kroovand and Perlmutter, 1981; Mehta et al., 2008; Turek et al., 1994; Zvizdic et al., 2009). Therefore, the mechanisms by which the Wolffian duct undergoes morphogenesis and the key factors that regulate this event were a focus of this study. In view of the importance of protein PTK7 towards morphogenesis of the cochlea and neural tube (Lu et al., 2004), and considering that PTK7 homologs off-track (Otk) and off-track 2 (Otk2) are required for morphogenesis of the ejaculatory duct and male fertility in Drosophila (Linnemannstons et al., 2014), PTK7 was hypothesized to be one of the major regulators of Wolffian duct morphogenesis. To this end, PTK7 conditional knockout mice were used to uncover the normal morphogenic events as well as understanding how Wolffian duct morphogenesis is regulated. The TCre-cKO provides an ideal model system for examining the regulation of Wolffian duct morphogenesis because the phenotype we observed was not due to androgen deficiency as shown by normal levels of androgen receptor and normal seminal vesicle weights.

Examination of intact Wolffian ducts from TCre-cKO and control mice clearly showed the importance of PTK7 towards maintaining proper morphogenesis of the Wolffian duct, which was essential for sperm motility, a key component of sperm maturation. These findings prompted us to focus on the cellular events that contribute to the morphogenesis of the Wolffian duct paying particular attention to the mechanisms by which the duct elongates and coils.

Cell division is a major mechanism by which tubes/ducts can elongate, but if cell division was the sole event, then the orientation of those divisions must be along the elongation axis. Although this is a major mechanism for elongation of kidney tubules (Karner et al., 2009; Yu et al., 2009), it was not for Wolffian duct elongation. Preferential orientation of the mitotic spindle along the elongation axis was not observed in the epithelium of the Wolffian duct. Therefore, other mechanisms are necessary to elongate the Wolffian duct.

Despite extensive elongation, the diameter of the Wolffian duct remained almost unchanged from embryonic (Hirashima, 2014) to early postnatal development (Fig. 2). As cell proliferation constantly adds cells to the epithelium, and random orientation of cell division contributes to both the length and diameter of the duct, it was hypothesized that CE-like cellular behavior occurs during Wolffian duct development to channel the increase in number of cells into an increase in overall length of the duct without an increase in diameter. Loss of Ptk7 did not affect cell proliferation, cell number increase, and cell division orientation. Rather, it resulted in a shorter and wider duct, which is an indication of disruption of CE. Therefore, a CE-like process occurs during morphogenesis of the Wolffian duct, and PTK7 is essential for this process.

The cellular mechanism of CE has been investigated in several model organisms (Walck-Shannon and Hardin, 2014). It is known that mediolateral intercalation within the same plane underlies CE. Mediolateral intercalation can be driven either by apical junction remodeling or mediolaterally biased basolateral protrusion activity (Walck-Shannon and Hardin, 2014; Williams et al., 2014). An ideal way to study intercalation is through tracking cell rearrangements over a time. Unfortunately, high resolution time-lapse imaging of living mammalian ductal structures remains challenging. However, we are able to infer some information about cell rearrangements by high-resolution imaging of freshly dissected ducts. Fig. 8 shows a stack of images from different focal planes of clusters of tall cells. At mid-levels of these cell clusters, rosette and T2 structures were observed; towards the apical direction, rosettes and T2 resolved along the elongation-axis while towards the basal direction, rosettes and T2 resolved mediolaterally. In some cells, apical regions of the cells were intercalated mediolaterally between two adjacent cells. These observations showed oriented cell rearrangements between basal and apical ends. Recently, it was reported that cell rearrangement behaviors were not synchronized at apical and basal ends of the epithelium of the mouse neural plate (Williams et al., 2014). Therefore, neighboring with different cells at basal and apical ends should not be surprising. However, oriented cell rearrangements at mid-levels have not been reported previously. Hypothetically, these rearrangements could be transient, i.e. cell intercalation with apical ends at a more advanced stage of this process and basal ends at a lag stage. In Ptk7 knockouts, epithelial cells rearranged in a random pattern at mid-levels. Likely, oriented cell rearrangements are another PCP characteristics and PTK7 has a role in regulating this behavior.

In most cases, mediolateral cell intercalation is regulated by PCP (Walck-Shannon and Hardin, 2014). A common feature of PCP-dependent mediolateral cell intercalation is that cells elongate perpendicular to the tissue extension axis within the plane of the epithelium (Karner et al., 2009; Williams et al., 2014). Another observation of PCP is polarized distribution of certain molecules such as PCP pathway components and cytoskeletal elements in the epithelium (Lienkamp et al., 2012; Williams et al., 2014). In this study, mediolateral polarization of the long axis of cells was observed at basal ends of epithelial cells, and polarized distribution of activated RLC of myosin II was found at basal ends and mid-levels of epithelial cells in the Wolffian duct. Loss of Ptk7 diminished both polarized cell elongation and polarized activity of myosin II. Therefore, our data demonstrate that epithelial cells of the Wolffian duct display PCP characteristics, which are regulated by PTK7.

PTK7 plays roles in cytoskeleton organization through regulating myosin II activity (Andreeva et al., 2014; Lee et al., 2012; Williams et al., 2014). In the Wolffian duct, the enriched activated RLC at the apical cell boundary of epithelial cells likely promoted apical constriction (Martin and Goldstein, 2014), which did not appear to be regulated by PTK7. In contrast, polarized enrichment of activated RLC at basal ends and mid-levels of epithelial cells aligned with cell elongation at basal ends and oriented cell rearrangements at mid-levels. Loss of Ptk7 diminished polarized RLC activity, which in turn disrupted the epithelial PCP characteristics such as oriented cell elongation and cell rearrangements, eventually resulting in a decrease in duct elongation and coiling. These findings were consistent with the inhibitor experiments. Inhibition of myosin II directly by blebbistatin or indirectly using

ROCK1/2 inhibitor Y27632 suppressed duct elongation and coiling. Therefore, PTK7 regulates PCP through regulating myosin activity and cytoskeleton organization, which in turn regulates Wolffian duct elongation and coiling.

Deletion of Ptk7 from smooth muscle cells surrounding the epithelium did not affect duct elongation and coiling. However, deletion of Ptk7 from epithelial cells resulted in dilation of the duct, suggesting epithelium-PTK7 autonomously regulates mediolateral intercalation of epithelial cells. Our two epithelial knockout models (RnCre-cKOs and HoxbCre-cKOs) showed milder defects compared to pan-mesoderm knockouts (TCre-cKOs). Rnase10-Cre removes genes from postnatal stage while Hoxb7-Cre removes genes in a mosaic pattern. Since the timing of deletion of Ptk7 is later in the Rnase10-Cre compared to the T-Cre deleted Ptk7, and the deletion of Ptk7 is mosaic in the epididymal epithelium when we use the Hoxb7-Cre, then it is not surprising that we observe a milder phenotype.

In a normal physiological condition, mediolateral intercalation of epithelial cells is concomitant with radial intercalation of mesenchymal cells in the Wolffian duct. During this process, the mesenchyme reduces its layers, and mesenchymal cells become more elongated. In the pan-mesoderm Ptk7 knockout, radial intercalation was affected as shown by additional layers of mesenchymal cells and the cells were not as elongated as controls (Fig. 2). This finding would suggest that PTK7 was required for radial intercalation. However, deletion of Ptk7 from smooth muscle cells using Sm22-Cre did not lead to morphological changes in the mesenchyme. Sm22-Cre becomes active around the time of smooth muscle appearance in the embryonic heart and the yolk sac at E8.5 (French et al., 2008; Miano et al., 2004). Recombination driven by Sm22-Cre is completed in smooth muscle of the Wolffian duct at E18.5 (Fig. S2). Deletion of Ptk7 using Sm22-Cre may not affect PCP in the mesenchyme if PCP is present prior to E18.5. Hence, a possible explanation for the lack of phenotype in SmCre-cKOs. Another possible explanation is that radial intercalation requires reorganization of extracellular matrix in the basement membrane of the epithelium (Walck-Shannon and Hardin, 2014). COL4 labeling at the basement membrane shows differences in Ptk7 knockouts compared to controls (Fig. 3E–F). This suggests that PTK7 may regulate extracellular matrix deposition, thereby indirectly regulating radial intercalation in the mesenchyme.

In conclusion, PTK7 regulates PCP through regulating myosin activity. PTK7-dependent PCP is required for cell intercalation and CE, which is essential for elongation and coiling of the Wolffian duct during tubular morphogenesis. This in turn allows for the proper development of a highly segmented organ of the proper shape and length for sperm maturation and male fertility.

4. Materials and Methods

4.1 Animals

Mice were handled according to the approved protocols following the guidelines of the Institutional Animal Care and Use Committee (IACUC) of the University of Virginia. Mice ($Ptk7^{flox/flox}$:mT/mG) carrying loxP-flanked Ptk7 allele and mT/mG (membrane-Tomato/membrane-EGFP) allele mated with mice ($Ptk7^{Xst87/+}$:T-$Cre^{tg/tg}$) carrying a disrupted allele

of Ptk7 gene, Xst87 (Lu et al., 2004), and two copies of T-Cre to generate conditional knockout ($Ptk7^{Xst87/flox}$:$T\text{-}Cre^{tg}$: mT/mG) and control offspring ($Ptk7^{+/flox}$:$T\text{-}Cre^{tg}$: mT/mG). In addition, $Ptk7^{flox/flox}$ mice mated with $Ptk7^{Xst87/+}$:$Hoxb7\text{-}Cre^{tg}$ mice to generate Hoxb7-Cre conditional knockouts ($Ptk7^{Xst87/flox}$:$Hoxb7\text{-}Cre^{tg}$). $Ptk7^{flox/flox}$ mice mated with $Ptk7^{Xst87/+}$:$Rnase10\text{-}Cre^{tg}$ mice to generate Rnase10-Cre conditional knockouts ($Ptk7^{Xst87/flox}$:$Rnase10\text{-}Cre^{tg}$). $Ptk7^{flox/flox}$ mice mated with $Ptk7^{Xst87/+}$:$Sm22\text{-}Cre^{tg}$ mice to generate Sm22-Cre conditional knockouts ($Ptk7^{Xst87/flox}$:$Sm22\text{-}Cre^{tg}$). Generation of Cre lines: Tg(Sm22-Cre) (Yoshida et al., 2010), Tg(Hoxb7-Cre) (Yu et al., 2002), and Tg(Rnase10-Cre) (Krutskikh et al., 2011) were reported previously. Mice were bred and genotyped based upon the information provided by The Jackson Laboratory (Bar Harbor, Maine).

4.2 Wolffian duct organ culture and inhibitor treatment

Embryos were dissected at 15.5 and 16.5 days post-coitum. Wolffian ducts were dissected free of the testes but the efferent ducts and the vas deferens remained. The ducts were cultured on a 0.4μm Millicell cell culture insert (Millipore, Billerica, MA) in DMEM/F12 medium containing 50ug/ml penicillin streptomycin, 1% ITS (insulin, transferin, and selenium) (Gibco, Langley, OK), and 10^{-8}M testosterone at 37°C with 5% CO_2. For blebbistatin inhibitor treatment experiments, E16.5 Wolffian ducts were incubated with DMSO or 2.5 to 5 μM blebbistatin, and then the images were taken at 0h, 5h, and 24h. Subsequently blebbistatin was removed, and the images were taken after 24h of inhibitor withdrawal. For Y27632 treatment experiments, E16.5 Wolffian ducts were incubated with DMSO or 1 to 2.5 μM Y27632, and then the images were taken at 0h, 24h, and 48h. Subsequently, Y27632 was removed, and the images were taken after 24h of inhibitor withdrawal.

4.3 Immunofluorescence

Epididymal tissue samples were immersion-fixed in 4% paraformaldehyde (PFA) in PBS (phosphate buffered saline) overnight at 4°C followed by paraffin embedding and sectioning. Knockout and control sections were placed on the same slide side by side to ensure similar treatment. Subsequently, slides were deparaffinized and rehydrated. For antigen retrieval, slides were microwaved in antigen unmasking solution (Vector Laboratories, Burlingame, CA) for 10 min on high in a 1300 W microwave and cooled for 1h at room temperature. Following blocking in blocking solution with 10% (v/v) normal goat or donkey serum (Vector Laboratories, Burlingame, CA), 0.5% (v/v) gelatin from cold-water fish skin (Sigma, St. Louis, MO), and TBS (tris-buffered saline) for 1.5h, slides were incubated overnight at 4°C in blocking solution with the primary antibodies. Following washing in TBS, slides were incubated with 1:200 dilution of Alexa Fluor 594 secondary antibodies (Molecular Probe, Eugene, OR) in blocking solution for 1.5h at room temperature. All slides were washed in TBS and mounted using Prolong Anti-fade reagent with DAPI for nuclear staining (Molecular Probe, Eugene, OR) and viewed under a Zeiss microscope equipped with epifluorescence. Two primary antibodies were purchased from Millipore (Billerica, MA): COL4 (collagen, type IV) antibody (#AB769, 1:200 working dilution) and phospho-histone H3 antibody (#06-570, 1:500 working dilution). Two antibodies were purchased from Santa Cruz Biotechnology (Santa Cruz, CA): atypical PKC (PKCζ) antibody (C-20)

(#sc-216, 1:200 working dilution) and AR antibody (H-280) (#sc-13062, 1:100 working dilution). CDH2 antibody was purchased from Epitomics (Burlingame, CA) (# 2019-1, 1:100 working dilution). Phospho-RLC antibody (#31694, 1:100 working dilution) was purchased from Rockland (Limerick, PA). An antibody against PTK7 ectodomain was described previously (Lu et al., 2004). α-tubulin antibody (#T9026, 1:250 working dilution) was from Sigma (St. Louis, MO), Cleaved-caspase3 antibody (#9661, 1:100 working dilution) was purchased from Cell Signaling Technology (Beverly, MA).

4.4 Whole mount immunofluorescence

E15.5 Wolffian ducts were fixed in 4% PFA at 4°C for 1–3h prior to washes in PBS at room temperature and permeabilized in tsPBS (0.5% Triton X-100 and 0.1% saponin in PBS) at 4°C overnight on a rocker. Samples were then incubated in a blocking solution (10% normal goat serum in tsPBS) for 1h at room temperature and then incubated overnight at 4°C in blocking solution with the primary antibodies. Following washing in tsPBS, slides were incubated with 1:200 dilutions of Alexa Fluor 594 secondary antibodies (Molecular Probe, Eugene, OR) in blocking solution overnight at 4°C. All samples were post-fixed in 4% PFA at 4°C for 0.5h and then washed and stored in PBS before imaging. Samples were then incubated in Sca/eA2 solution (4M urea, 10% glycerol, and 0.1% Triton X-100) (Hama et al., 2011) for at least 0.5h before visualizing under a Zeiss 780 confocal microscope. Primary antibodies included phosphohistone H3 antibody (#06-570, 1:200 working dilution) from Millipore (Billerica, MA) and phospho-RLC antibody (#31694, 1:100 working dilution) from Rockland (Limerick, PA). ImageJ (www.imagej.nih.gov) was used to measure labeling intensity at the cell boundary. Briefly, a square area was selected to include a section of a cell boundary. The intensity of the area vs. the length of the cell boundary was assigned as labeling intensity of that cell boundary. The same square was then moved to measure other boundaries.

4.5 Measurement of the orientation of cell division

E15.5 Wolffian ducts were labeled with anti-phospho-histone H3 antibody. 3D reconstructions of Z-stack images of these ducts were generated using Volocity 6.3 (PerkinElmer, Waltham, MA) software. Cell division angles were measured according to a protocol reported previously (Yu et al., 2009). Briefly, the poles of each of the two anaphase chromosome clusters in 3D reconstructions were marked as measurement points P1 and P2. The x, y and z coordinates of the two points were acquired for generation of the vector of the mitotic division axis. Two points (P3, P4) along the duct axis of a straight E15.5 Wolffian duct were taken to generate the vector of the elongation axis (Fig. S3A). The coordinates of the four points were used to calculate the angles between the vector of the mitotic division axis and the vector of the elongation axis. P14 Wolffian ducts were labeled with an antibody against α-tubulin and the orientation of mitotic spindles was measured (Fig. S3B–I).

4.6 Cell shape measurement and cell rearrangement analysis

To study the shape of epithelial cells, we took advantage of mGmT allele which had already been inserted into the genome of control ($Ptk7^{flop/+}$:T-Cre^{tg}: mGmT) and TCre-cKO ($Ptk7^{flop/Xst87}$: T-Cre^{tg}: mGmT) mice (Williams et al., 2014). In these mice, epididymal cells possessed EGFP labeling at the cell membrane, which outlined the shape of cells. The

Wolffian ducts freshly dissected from E18.5 mice were incubated in a culture medium described above at 37°C with 5% CO_2. Confocal imaging was preformed using a Zeiss 780 confocal microscope. A section of the duct, whose axis lay on the XY plane, was selected, and then Z-stacks (1μm steps, captured at 40×, 1024 × 1024 pixels at 0.208 μm/pixel) were captured.

ImageJ (www.imagej.nih.gov) and Volocity 6.3 (PerkinElmer, Waltham, MA) software were used for image analyses. To measure the height of epithelial cells and lumen diameter of the Wolffian duct, an XY plane across the center of a Wolffian duct was selected. The length of the lines, which were drawn from the apical to basal membrane of epithelial cells, was measured as the height of epithelial cells. Luminal diameter was measured using ImageJ software. An average of 3–5 measurements were recorded. An epithelial cell with its apical to basal axis perpendicular to the XY plane was selected for measurement. Therefore, a cell was selected only if the distance from the basal section to apical section of the cell equaled to the height of the cell. To study cell elongation at basal ends of epithelial cells, the basal section of selected cells was identified, and two roughly parallel lines were drawn on opposite sides of each cell. The distance between parallel lines was measured, and then a length to width ratio was assigned to each individual cell, with the length being the longer of the two sides. Cells that had a length to width ratio of greater than 1.2 were considered elongated (Karner et al., 2009). The angle between the elongated axis of the cell and the elongated axis of the Wolffian duct was measured using ImageJ (www.imagej.nih.gov). The percentage of total cells that fell into each 10 degrees was recorded. Similar elongation measurements were performed for the cellular apical region.

Cell rearrangements were analyzed using the terminology reported previously (Williams et al., 2014). As shown in Fig. S4A, a T1 process involves a cluster of four cells that transit among a neighbor contact along the elongation axis (T1), a four-cell vertex (T2), and a mediolateral neighbor contact (T3). Rosette resolution involves a cluster of five or more cells that transit among an elongation-axis-oriented array (E), a rosette (R), and a mediolateral oriented array (M). A single cell intercalation involves the apical region of a single cell intercalating between two neighbors that lay either along the elongation axis (Y) or along the circumference of the duct (X).

4.7 Statistics

One way analysis-of-variance (ANOVA) was performed to identify significant differences of means. Significant differences were indicated by * ($p<0.05$) and ** ($p<0.01$). Kolmogorov-Smirnov (KS) tests were performed to determine whether cell division orientation was random and whether cell elongation orientation were significantly different between controls and TCrecKOs using IBM SPSS software.

Supplementary Material

Refer to Web version on PubMed Central for supplementary material.

Acknowledgments

We thank Yuesheng Li, Hameeda Naimi, and Akwasi Asante for their assistance in performing experiments. We thank Dr. Mark Lewandoski at National Cancer Institute for the T-Cre mouse line. This work was supported by Eunice Shriver National Institute of Child Health and Human Development/NIH Grant RO1-HD069654 (BTH), R01-DC013773 (XL), FAPESP-2014/23382-9 (RFD) and CAPES-BEX 5874/14-9 (ACFS).

References

Andreeva A, Lee J, Lohia M, Wu X, Macara IG, Lu X. PTK7-Src signaling at epithelial cell contacts mediates spatial organization of actomyosin and planar cell polarity. Developmental cell. 2014; 29:20–33. [PubMed: 24703874]

Andrew DJ, Ewald AJ. Morphogenesis of epithelial tubes: Insights into tube formation, elongation, and elaboration. Developmental biology. 2010; 341:34–55. [PubMed: 19778532]

Carroll TJ, Yu J. The kidney and planar cell polarity. Current topics in developmental biology. 2012; 101:185–212. [PubMed: 23140630]

French WJ, Creemers EE, Tallquist MD. Platelet-derived growth factor receptors direct vascular development independent of vascular smooth muscle cell function. Molecular and cellular biology. 2008; 28:5646–5657. [PubMed: 18606782]

Girgis SM, Etriby AN, Ibraim AA, Kahil SA. Testicular biopsy in azoospermia. A review of the last ten years' experiences of over 800 cases. Fertil Steril. 1969; 20:467–477. [PubMed: 5769396]

Hama H, Kurokawa H, Kawano H, Ando R, Shimogori T, Noda H, Fukami K, Sakaue-Sawano A, Miyawaki A. Scale: a chemical approach for fluorescence imaging and reconstruction of transparent mouse brain. Nature neuroscience. 2011; 14:1481–1488. [PubMed: 21878933]

Hayes M, Naito M, Daulat A, Angers S, Ciruna B. Ptk7 promotes non-canonical Wnt/PCP-mediated morphogenesis and inhibits Wnt/beta-catenin-dependent cell fate decisions during vertebrate development. Development. 2013; 140:1807–1818. [PubMed: 23533179]

Hinton BT, Galdamez MM, Sutherland A, Bomgardner D, Xu B, Abdel-Fattah R, Yang L. How do you get six meters of epididymis inside a human scrotum? J Androl. 2011; 32:558–564. [PubMed: 21441421]

Hirashima T. Pattern formation of an epithelial tubule by mechanical instability during epididymal development. Cell reports. 2014; 9:866–873. [PubMed: 25437543]

Iruela-Arispe ML, Beitel GJ. Tubulogenesis. Development. 2013; 140:2851–2855. [PubMed: 23821032]

Karner CM, Chirumamilla R, Aoki S, Igarashi P, Wallingford JB, Carroll TJ. Wnt9b signaling regulates planar cell polarity and kidney tubule morphogenesis. Nature genetics. 2009; 41:793–799. [PubMed: 19543268]

Kobayashi A, Kwan KM, Carroll TJ, McMahon AP, Mendelsohn CL, Behringer RR. Distinct and sequential tissue-specific activities of the LIM-class homeobox gene Lim1 for tubular morphogenesis during kidney development. Development. 2005; 132:2809–2823. [PubMed: 15930111]

Kroovand, R.; Perlmutter, A. Congenital anomalies of the vas deferens and epididymis. In: Kogan, SJ.; Hafez, ESE., editors. Pediatric Andrology. Boston: Martinus Nijhoff Publishers; 1981. p. 173-180.

Krutskikh A, De Gendt K, Sharp V, Verhoeven G, Poutanen M, Huhtaniemi I. Targeted inactivation of the androgen receptor gene in murine proximal epididymis causes epithelial hypotrophy and obstructive azoospermia. Endocrinology. 2011; 152:689–696. [PubMed: 21084446]

Lee J, Andreeva A, Sipe CW, Liu L, Cheng A, Lu X. PTK7 regulates myosin II activity to orient planar polarity in the mammalian auditory epithelium. Current biology : CB. 2012; 22:956–966. [PubMed: 22560610]

Lienkamp SS, Liu K, Karner CM, Carroll TJ, Ronneberger O, Wallingford JB, Walz G. Vertebrate kidney tubules elongate using a planar cell polarity-dependent, rosette-based mechanism of convergent extension. Nature genetics. 2012; 44:1382–1387. [PubMed: 23143599]

Linnemannstons K, Ripp C, Honemann-Capito M, Brechtel-Curth K, Hedderich M, Wodarz A. The PTK7-Related Transmembrane Proteins Off-track and Off-track 2 Are Co-receptors for Drosophila Wnt2 Required for Male Fertility. PLoS genetics. 2014; 10:e1004443. [PubMed: 25010066]

Lu X, Borchers AG, Jolicoeur C, Rayburn H, Baker JC, Tessier-Lavigne M. PTK7/CCK-4 is a novel regulator of planar cell polarity in vertebrates. Nature. 2004; 430:93–98. [PubMed: 15229603]

Lubarsky B, Krasnow MA. Tube morphogenesis: making and shaping biological tubes. Cell. 2003; 112:19–28. [PubMed: 12526790]

Martin AC, Goldstein B. Apical constriction: themes and variations on a cellular mechanism driving morphogenesis. Development. 2014; 141:1987–1998. [PubMed: 24803648]

Mehta GU, Shively SB, Duong H, Tran M, Moncrief TJ, Smith JH, Li J, Edwards NA, Lonser RL, Zhuang Z, Merrill MJ, Raffeld M, Maxwell P, Oldfield EH, Vortmeyer AO. Progression of epididymal maldevelopment into hamartoma-like neoplasia in VHL disease. Neoplasia. 2008; 10:1146–1153. [PubMed: 18813354]

Miano JM, Ramanan N, Georger MA, de Mesy Bentley KL, Emerson RL, Balza RO Jr, Xiao Q, Weiler H, Ginty DD, Misra RP. Restricted inactivation of serum response factor to the cardiovascular system. Proceedings of the National Academy of Sciences of the United States of America. 2004; 101:17132–17137. [PubMed: 15569937]

Mugford JW, Sipila P, Kobayashi A, Behringer RR, McMahon AP. Hoxd11 specifies a program of metanephric kidney development within the intermediate mesoderm of the mouse embryo. Developmental biology. 2008; 319:396–405. [PubMed: 18485340]

Perantoni AO, Timofeeva O, Naillat F, Richman C, Pajni-Underwood S, Wilson C, Vainio S, Dove LF, Lewandoski M. Inactivation of FGF8 in early mesoderm reveals an essential role in kidney development. Development. 2005; 132:3859–3871. [PubMed: 16049111]

Schnell U, Carroll TJ. Planar cell polarity of the kidney. Experimental cell research. 2014 http://dx.doi.org/10.1016/j.yexcr.2014.11.003.

Sun EL, Flickinger CJ. Proliferative activity in the rat epididymis during postnatal development. Anat Rec. 1982; 203:273–284. [PubMed: 7202338]

Turek PJ, Ewalt DH, Snyder HM, Duckett JW. Normal Epididymal Anatomy in Boys. J Urology. 1994; 151:726–727.

Vicente-Manzanares M, Ma X, Adelstein RS, Horwitz AR. Non-muscle myosin II takes centre stage in cell adhesion and migration. Nature reviews. Molecular cell biology. 2009; 10:778–790. [PubMed: 19851336]

Walck-Shannon E, Hardin J. Cell intercalation from top to bottom. Nature reviews. Molecular cell biology. 2014; 15:34–48. [PubMed: 24355988]

Wilkinson S, Paterson HF, Marshall CJ. Cdc42-MRCK and Rho-ROCK signalling cooperate in myosin phosphorylation and cell invasion. Nature cell biology. 2005; 7:255–261. [PubMed: 15723050]

Williams M, Yen W, Lu X, Sutherland A. Distinct apical and basolateral mechanisms drive planar cell polarity-dependent convergent extension of the mouse neural plate. Developmental cell. 2014; 29:34–46. [PubMed: 24703875]

Xu B, Yang L, Hinton BT. The Role of fibroblast growth factor receptor substrate 2 (FRS2) in the regulation of two activity levels of the components of the extracellular signal-regulated kinase (ERK) pathway in the mouse epididymis. Biol Reprod. 2013; 89:48. [PubMed: 23782834]

Xu B, Yang L, Lye RJ, Hinton BT. p-MAPK1/3 and DUSP6 regulate epididymal cell proliferation and survival in a region-specific manner in mice. Biol Reprod. 2010; 83:807–817. [PubMed: 20650883]

Xu BF, Washington AM, Hinton BT. PTEN signaling through RAF1 proto-oncogene serine/threonine kinase (RAF1)/ERK in the epididymis is essential for male fertility. Proceedings of the National Academy of Sciences of the United States of America. 2014; 111:18643–18648. [PubMed: 25512490]

Yen WW, Williams M, Periasamy A, Conaway M, Burdsal C, Keller R, Lu X, Sutherland A. PTK7 is essential for polarized cell motility and convergent extension during mouse gastrulation. Development. 2009; 136:2039–2048. [PubMed: 19439496]

Yoshida T, Gan Q, Franke AS, Ho R, Zhang J, Chen YE, Hayashi M, Majesky MW, Somlyo AV, Owens GK. Smooth and cardiac muscle-selective knock-out of Kruppel-like factor 4 causes

postnatal death and growth retardation. The Journal of biological chemistry. 2010; 285:21175–21184. [PubMed: 20439457]

Yu J, Carroll TJ, McMahon AP. Sonic hedgehog regulates proliferation and differentiation of mesenchymal cells in the mouse metanephric kidney. Development. 2002; 129:5301–5312. [PubMed: 12399320]

Yu J, Carroll TJ, Rajagopal J, Kobayashi A, Ren Q, McMahon AP. A Wnt7b-dependent pathway regulates the orientation of epithelial cell division and establishes the cortico-medullary axis of the mammalian kidney. Development. 2009; 136:161–171. [PubMed: 19060336]

Zvizdic Z, Huskic J, Dizdarevic S, Karavdic K, Zvizdic D. Incidence of epididymal disjunction anomalies associated with an undescended testis. Folia Med. 2009; 44:65–68.

Highlights

- Planar cell polarity and cell rearrangements drive Wolffian duct morphogenesis.
- PTK7 regulates PCP and unique cell rearrangements necessary for convergent extension.
- Polarized activity of myosin underlies convergent extension cell rearrangements.
- Cell division orientation along the ductal axis is random, and not regulated by POTK7.
- PTK7 maintains proper WD morphogenesis, which is necessary for sperm maturation.

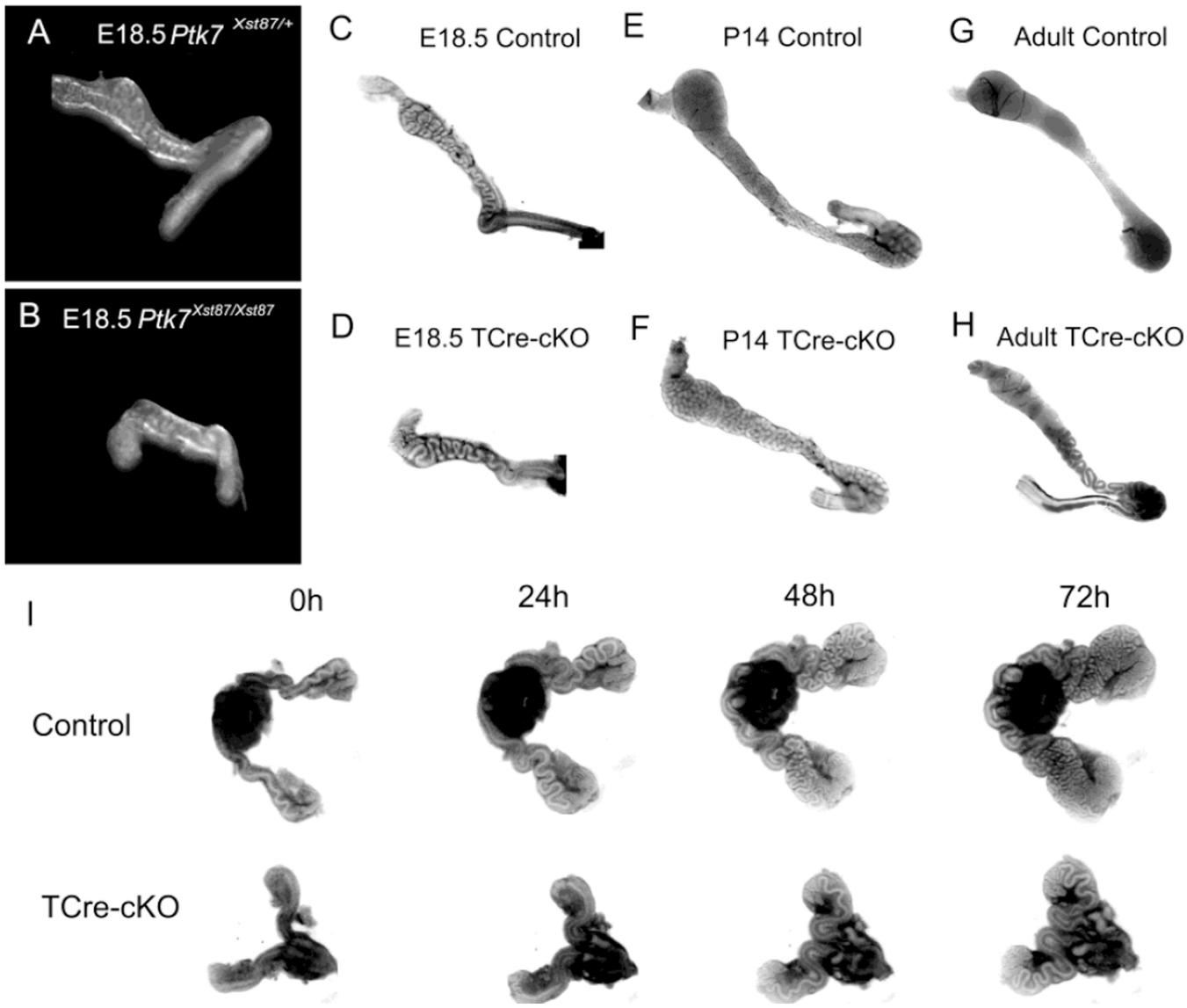

Fig. 1.

Abnormal elongation and coiling in Ptk7 mutant Wolffian ducts. (A–B) E18.5 $Ptk7^{Xst87/+}$ and $Ptk7^{Xst87/Xst87}$ Wolffian ducts. (C–D) E18.5 control and TCre-cKO Wolffian ducts. (E–F) P14 control and TCre-cKO ducts. (G–H) Adult control and TCre-cKO Wolffian ducts. (I) 72h of organ culture of E15.5 Wolffian ducts from controls and TCre-cKOs.

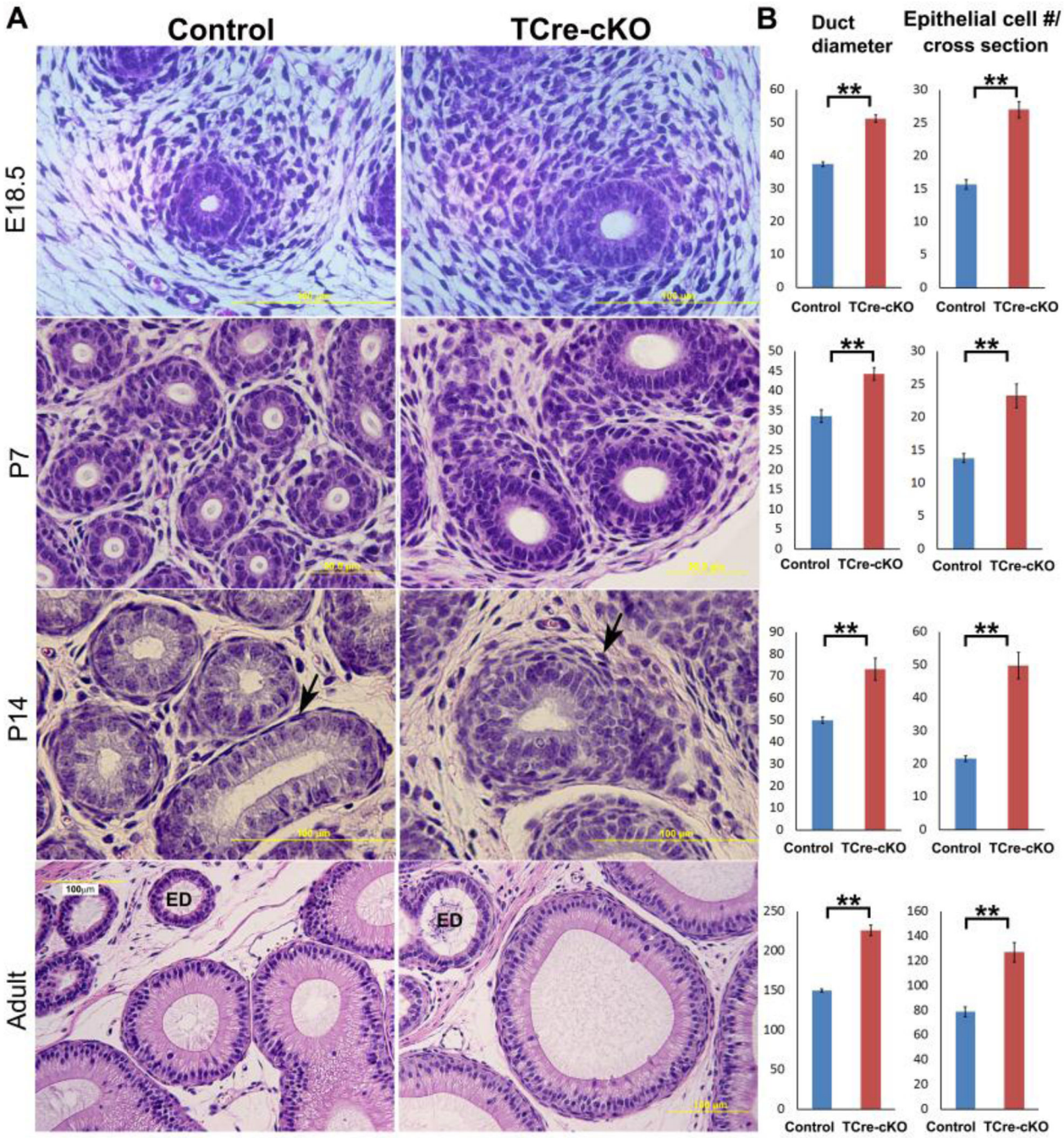

Fig. 2.

Morphological differences between control and TCre-cKO Wolffian ducts. (A) Proximal regions of control and TCre-cKO Wolffian ducts at E18.5, P7, P14, and adults. (B) Statistical analysis of diameter and number of epithelial cells per cross-section of Wolffian ducts in TCre-cKOs and controls. n ≥ 3. Data are presented as mean ± SEM. ** $p<0.01$.

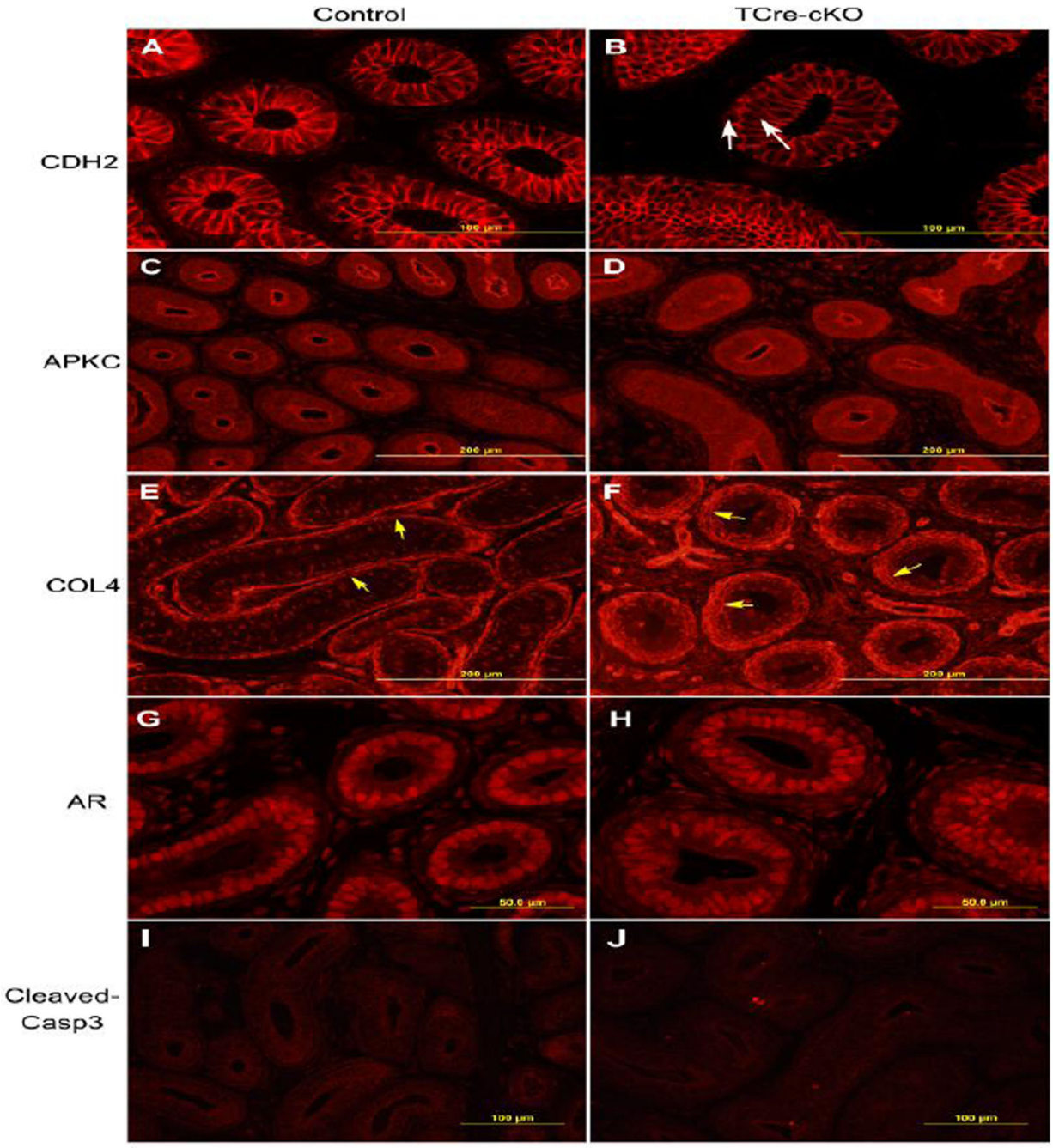

Fig. 3.

Identification of adhesion junctions, apical-basal polarity, basement membranes, AR localization, and apoptotic cells in the control and TCre-cKO epithelium at P14. (A–B) Representative images of localization of adhesion junction component CDH2 in controls and TCre-cKOs. White arrows show pseudostratified epithelial cells. (C–D) Representative images of apical localization of atypical PKC (APKC) in controls and TCre-cKOs. (E–F) Representative images of COL4 localization in controls and TCre-cKOs. Yellow arrows show the basement membrane. (G–H) Representative images of AR localization in controls

and TCre-cKOs. (I–J) Representative images of cleaved caspase3 localization in controls and TCre-cKOs.

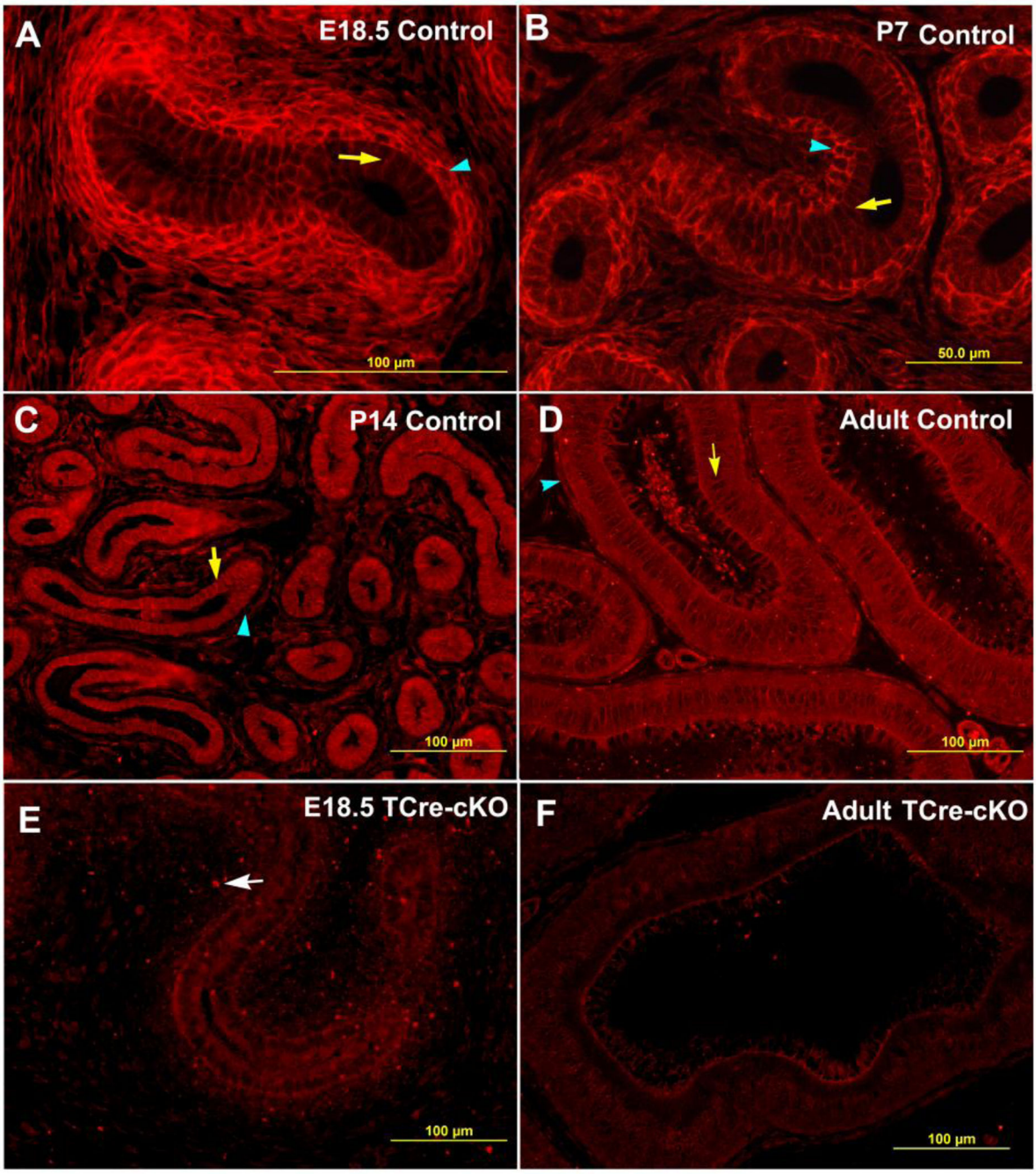

Fig. 4.

Changes of PTK7 localization during Wolffian duct development. Representative images show PTK7 immunolocalization in control proximal Wolffian ducts at E18.5 (A), P7 (B), P14 (C), adults (D), and in TCre-cKO proximal Wolffian ducts at E18.5 (E) and adults (F), respectively. Yellow arrows show epithelial cells. Blue arrowheads show mesenchymal cells surrounding the epithelium. The white arrow points to punctate labeling from the gene trap mutant Ptk7 allele (Xst87).

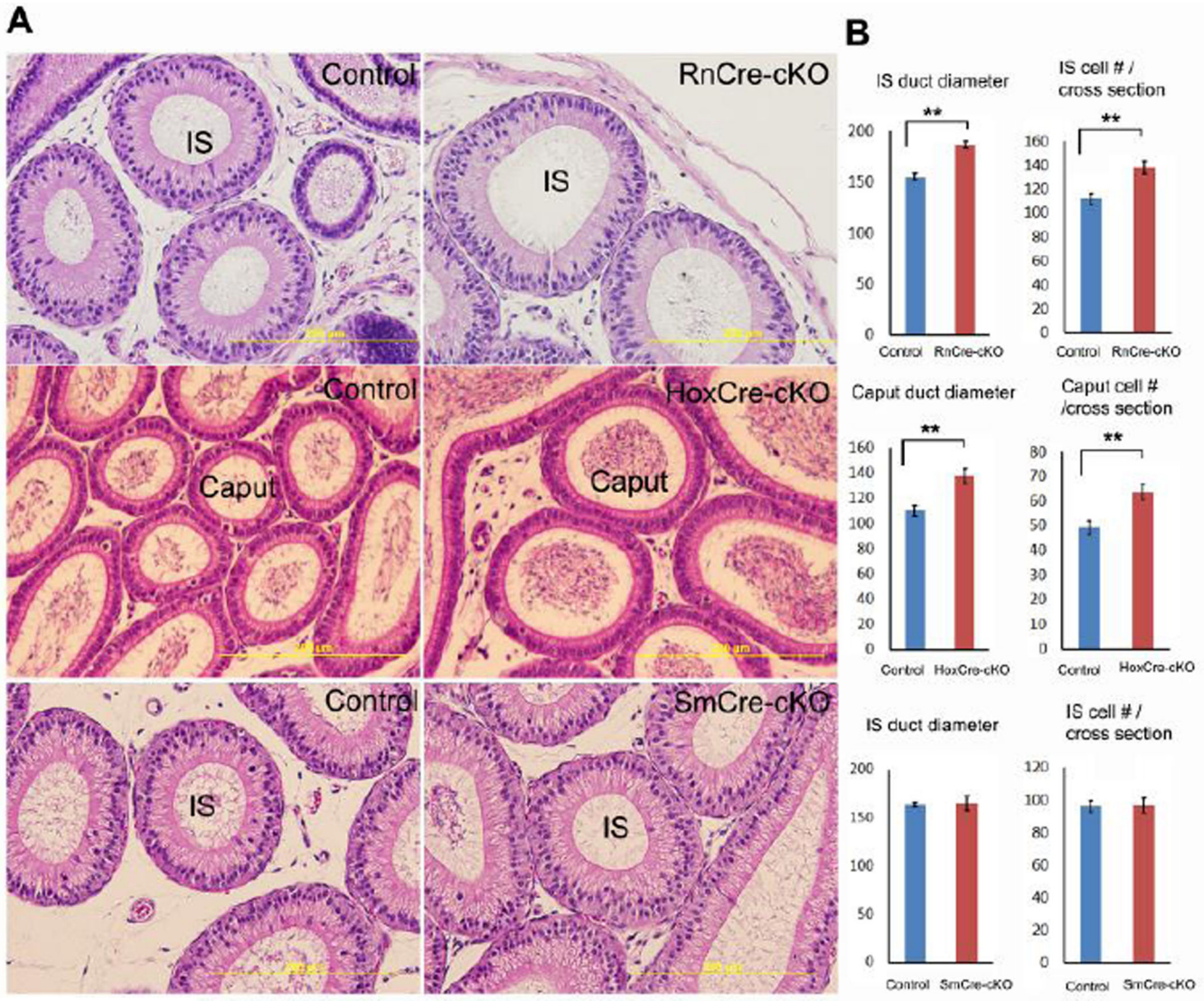

Fig. 5.

Morphological changes in adult epididymal ducts of three Ptk7 conditional knockouts (RnCre-cKO, HoxCre-cKO, and SmCre-cKO). (A) Representative images of epididymal ducts in the initial segment (IS) or caput of three Ptk7 conditional knockouts and corresponding controls. (B) Statistical analysis of duct diameter and epithelial cell number per cross-section in three Ptk7 conditional knockouts and controls. $n \geq 3$. Data are presented as mean ± SEM. ** $p<0.01$.

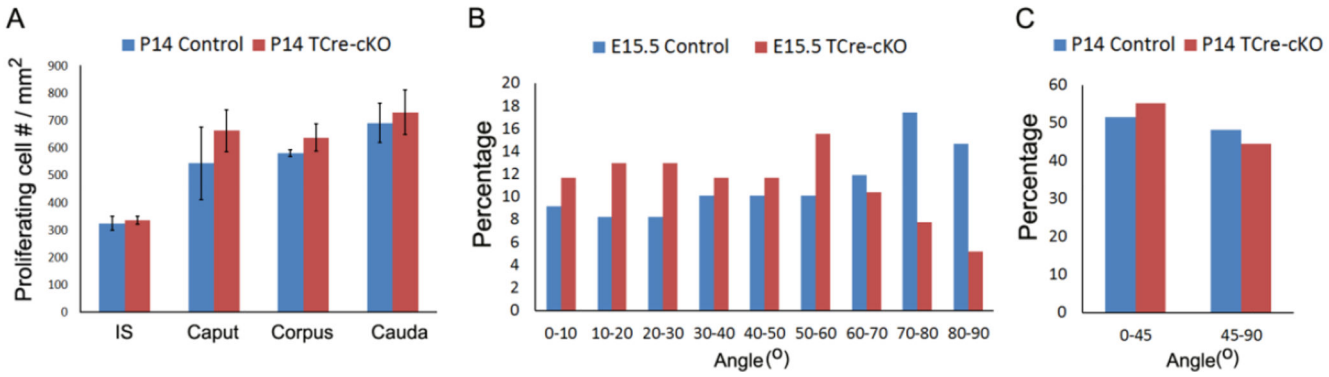

Fig. 6.

Cell proliferation and division orientation of epithelial cells in control and TCre-cKO Wolffian ducts. (A) Comparison of cell proliferation between TCre-cKOs and controls in the epithelium of each epididymal region at P14. (B) Measurement of cell division orientation of epithelial cells in E15.5 controls and TCre-cKOs. The total number of dividing cells measured is 109 and 77 for E15.5 controls and TCre-cKOs, respectively. (C) Analysis of cell division orientation of epithelial cells in P14 controls and TCre-cKOs. The total number of dividing cells analyzed is 453 and 121 for P14 controls and TCre-cKOs, respectively. Data are presented as mean ± SEM.

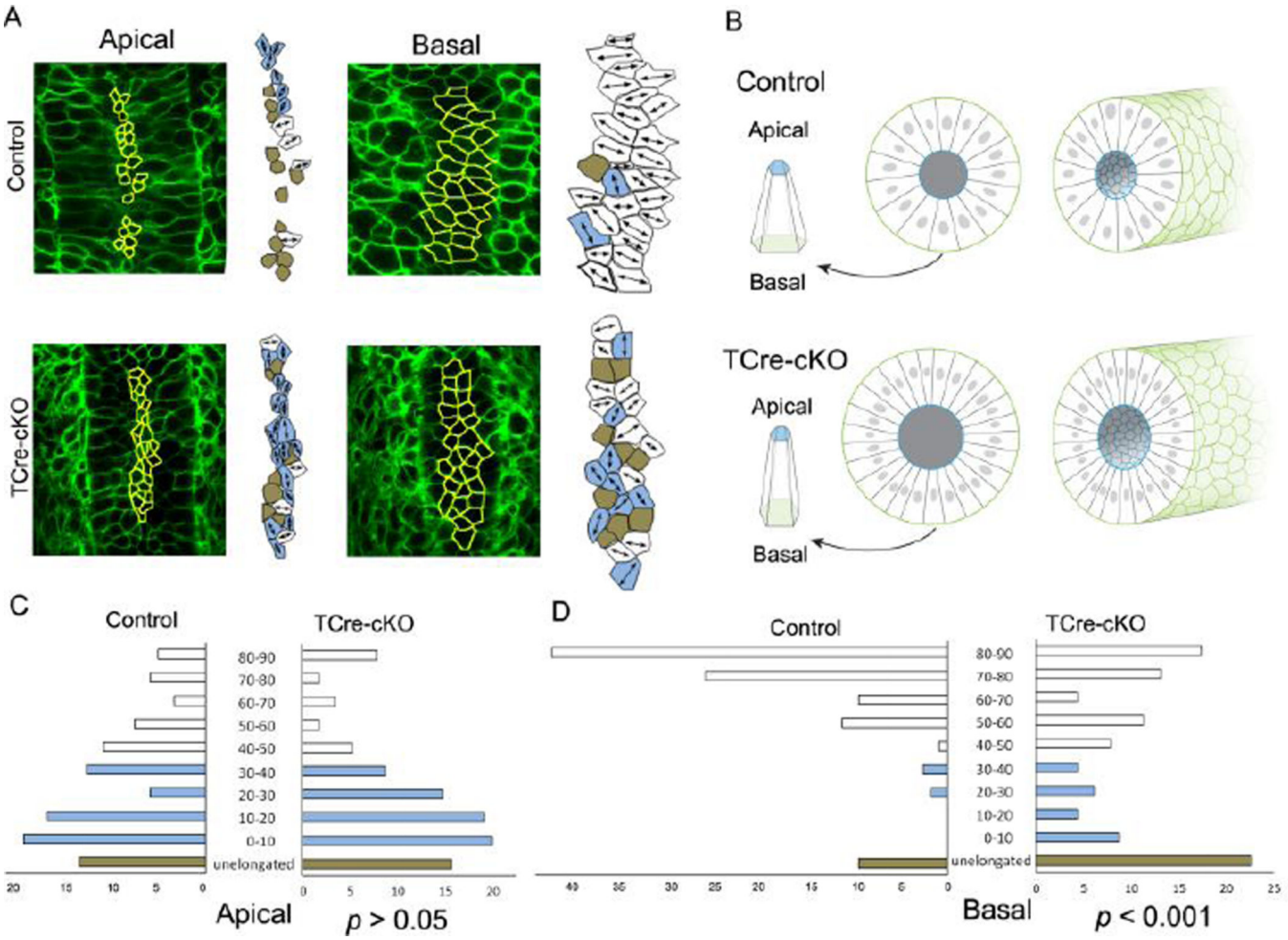

Fig. 7.

Elongation and alignment of epithelial cells in controls and TCre-cKOs. (A) Confocal images and outlines of epithelial cells at apical and basal ends (yellow line) in E18.5 controls and TCre-cKOs, respectively. Mediolaterally elongated cells are marked in white, cells elongated along the duct axis are marked in light blue, and unelongated cells are marked in brown. (B) 3D diagrams of representative epithelial cells, cross-sections and 3D diagrams of Wolffian duct sections of controls and TCre-cKOs, respectively. (C) Quantitation of cellular elongation angle relative to the duct axis at apical ends of epithelial cells in E18.5 controls and TCre-cKOs. There is no significant change in the orientation of the elongated cells at apical ends between controls and TCre-cKOs ($p>0.05$, KS test). (D) Quantitation of cellular elongation angle relative to the duct axis at basal ends of epithelial cells in E18.5 controls and TCre-cKOs. There is a significant change in the orientation of the elongated cells at basal ends between controls and TCre-cKOs ($p<0.001$, KS test). White bars show cells that elongate perpendicular to the elongation axis (45–90°). Light blue bars represent cells that elongate parallel (0–45°). Brown bars represent cells that are unelongated. The data were generated from at least 4 different animals. The total number of cells measured is 118 and 114 for controls and TCre-cKOs, respectively.

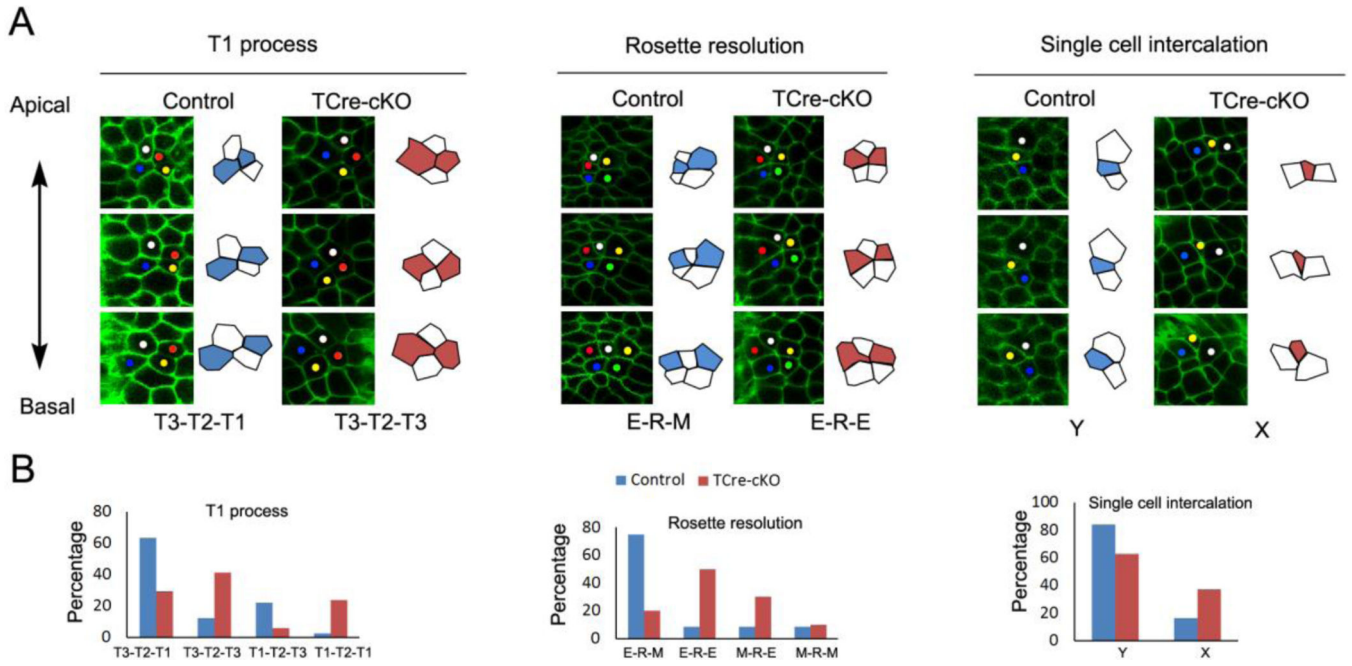

Fig. 8.

Cell rearrangements at mid-levels of epithelial cells. (A) Confocal images and outlines of cell clusters showing the common types of cell rearrangements of T1 process, rosette resolution, and single cell intercalation from the apical to basal direction in controls and TCre-cKOs. The y-axis of the images is parallel to the elongation axis. (B) Frequency of each type of cell rearrangements. The data were generated from at least 4 different animals. The total number of cell clusters analyzed in controls and TCre-cKOs for T1 process is 41, 17, for rosette resolution is 12, 11, for single cell intercalation is 37, 27, respectively.

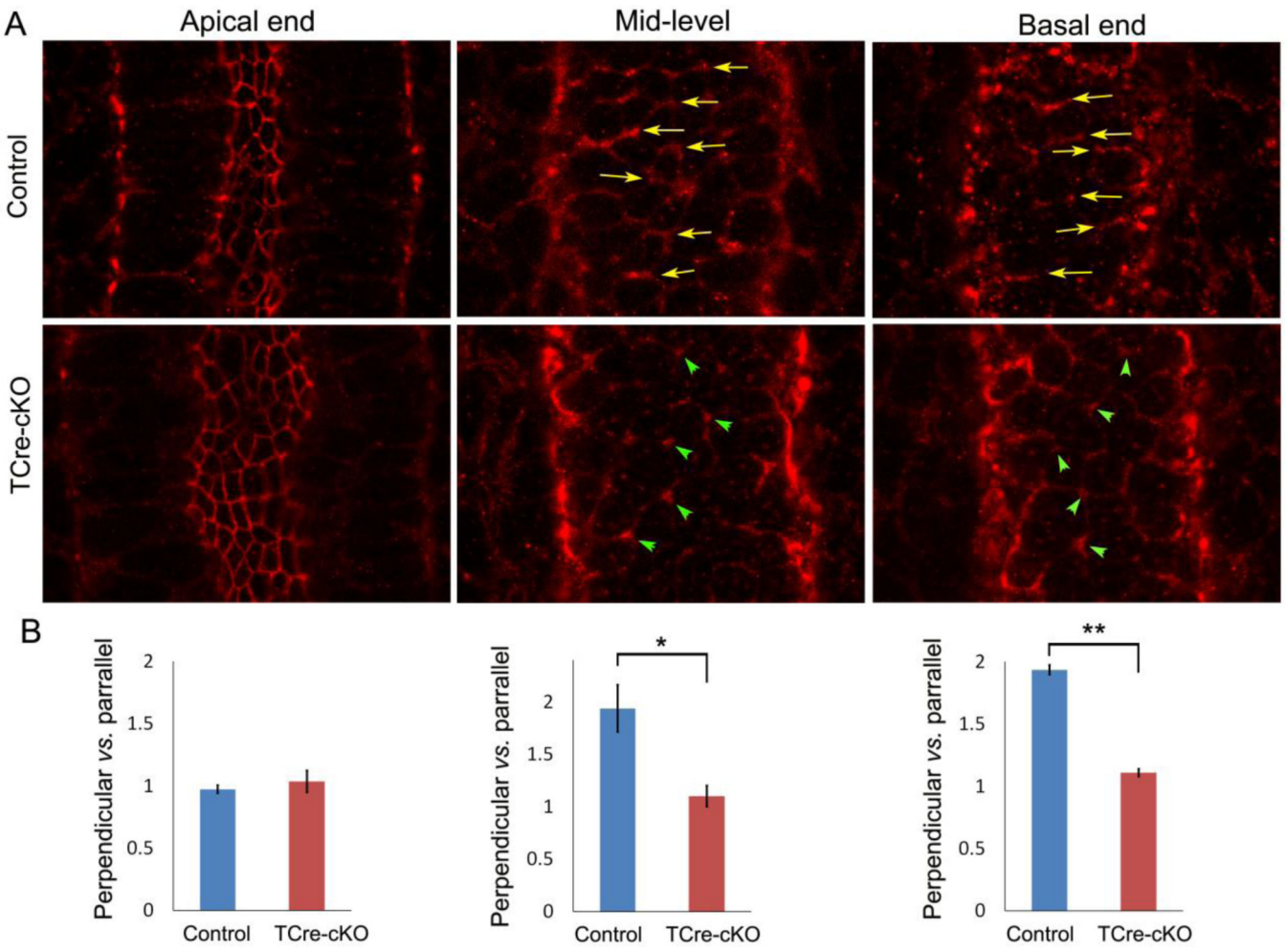

Fig. 9.

Localization of phosphorylated myosin regulatory light chain (pRLC) in controls and TCre-cKOs. (A) Localization of pRLC at apical ends, mid-levels, and basal ends of epithelial cells in E15.5 controls and TCre-cKOs. Arrows show preferential pRLC localization at the cell boundary perpendicular to the axis of the duct. Arrowheads show pRLC localization at the points where several cell boundaries join. (B) Statistical analysis of labeling intensity at the cell boundaries perpendicular vs. parallel to the duct axis. $n \geq 3$. Data are presented as mean ± SEM. ** $p<0.01$; * $p<0.05$.

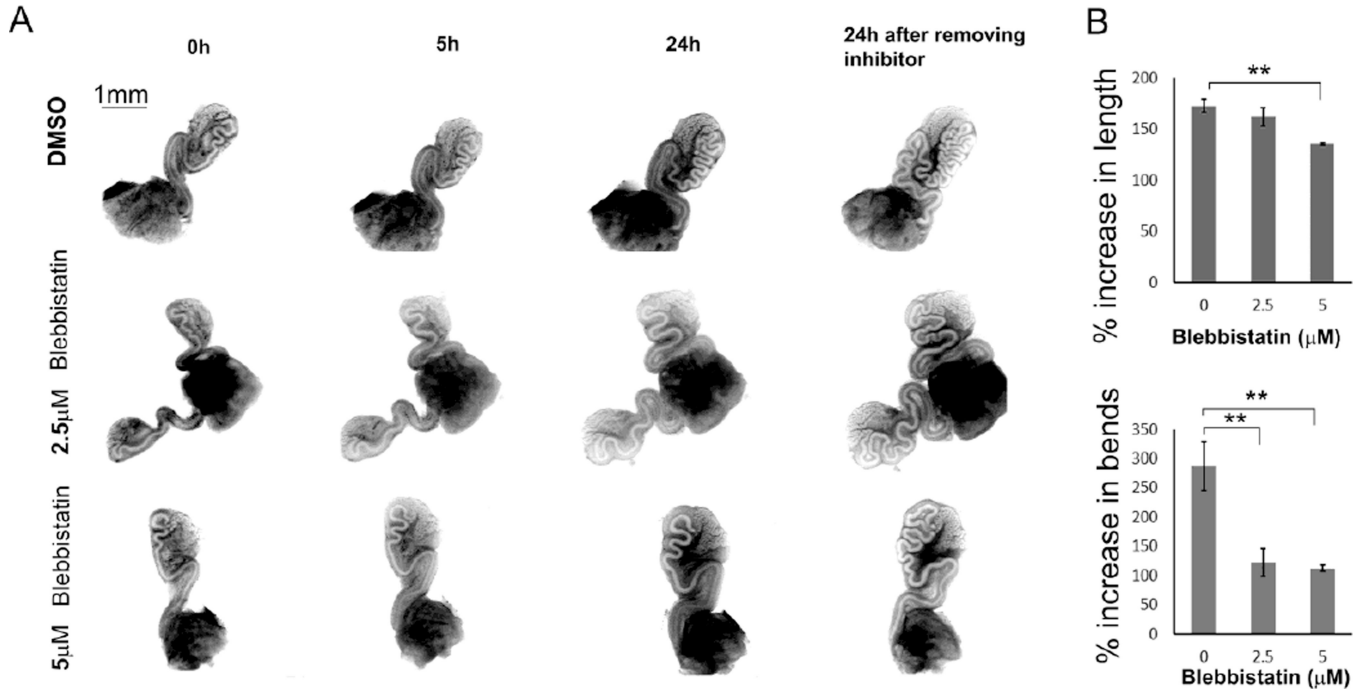

Fig. 10.

Inhibitory effect of blebbistatin on elongation and coiling of Wolffian ducts. (A) Decreased elongation and coiling when E16.5 wild-type Wolffian ducts were incubated with 2.5 μM or 5 μM blebbistatin compared to DMSO controls. The images were taken at 0h, 5h, and 24h. After 24h culture, blebbistatin was removed, and the images were recorded after 24h of inhibitor withdrawal. (B) Statistical analysis of elongation and coiling of Wolffian ducts during the first 24h of incubation with blebbistatin. $n \geq 3$. Data are presented as mean ± SEM. ** $p<0.01$.

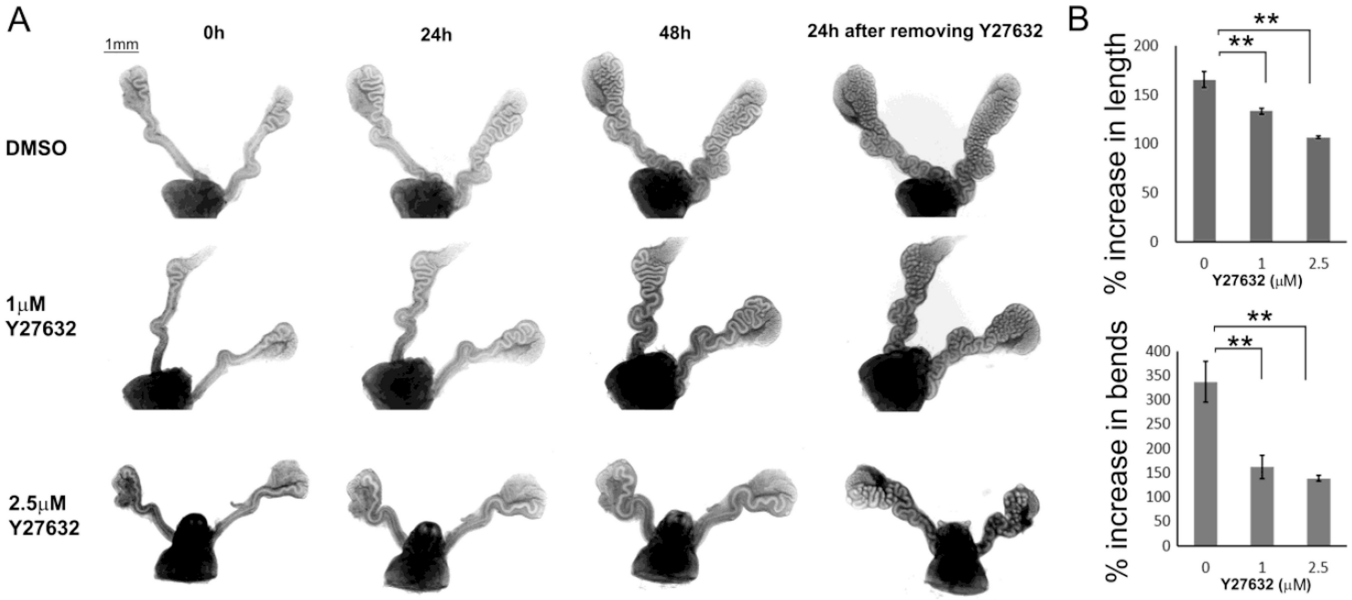

Fig. 11.

Inhibitory effects of Y27632 on elongation and coiling of Wolffian ducts. (A) Decreased elongation and coiling when E16.5 wild-type Wolffian ducts were incubated with 1μM or 2.5μM Y27632 compared to DMSO controls. The images were recorded at 0h, 24h, and 48h. Y27632 was then removed, and the images were taken after 24h of inhibitor withdrawal. (B) Statistical analysis of elongation and coiling of Wolffian ducts during the first 24h of incubation with Y27632. A curve, which has an angle less than 60 degree, is considered as a bend. $n \geq 3$. Data are presented as mean ± SEM. ** $p<0.01$.